Near-Quantum-Noise Axion Dark Matter Search at CAPP around 9.5 μeV

Jinsu Kim,[1,2] Ohjoon Kwon,[2] Çağlar Kutlu,[1,2] Woohyun Chung,[2,*] Andrei Matlashov,[2] Sergey Uchaikin,[2] Arjan Ferdinand van Loo,[3,4] Yasunobu Nakamura,[4] Seonjeong Oh,[2] HeeSu Byun,[2] Danho Ahn,[1,2] and Yannis K. Semertzidis[2,1]

[1]*Department of Physics, KAIST, Daejeon 34141, Republic of Korea*
[2]*Center for Axion and Precision Physics Research (CAPP), IBS, Daejeon 34051, Republic of Korea*
[3]*RIKEN Center for Quantum Computing (RQC), Wako, Saitama 351–0198, Japan*
[4]*Department of Applied Physics, Graduate School of Engineering, The University of Tokyo, Bunkyo-ku, Tokyo 113-8656, Japan*

(Received 9 August 2022; accepted 19 January 2023; published 28 February 2023)

We report the results of an axion dark matter search over an axion mass range of 9.39–9.51 μeV. A flux-driven Josephson parametric amplifier (JPA) was added to the cryogenic receiver chain. A system noise temperature of as low as 200 mK was achieved, which is the lowest recorded noise among published axion cavity experiments with phase-insensitive JPA operation. In addition, we developed a two-stage scanning method which boosted the scan speed by 26%. As a result, a range of two-photon coupling in a plausible model for the QCD axion was excluded with an order of magnitude higher in sensitivity than existing limits.

DOI: 10.1103/PhysRevLett.130.091602

Axions, hypothetical particles associated with the spontaneous breaking of a postulated global U(1) symmetry, offer a dynamic solution to the strong *CP* problem, an important puzzle in the standard model (SM) [1]. Axions in the mass range of 1 μeV–10 meV are considered a favored candidate for dark matter [2,3], but they have extremely weak interactions with the SM fields [4,5], which makes relevant searches exceptionally difficult. To date, Sikivie's haloscope remains the most sensitive approach in this mass range [6]. Relying on the two-photon coupling that converts an axion into a single photon, it utilizes a frequency-tunable microwave cavity immersed in a strong magnetic field.

One of the most effective tools for improving the haloscope's performance is the quantum-noise-limited amplifier, which was successfully developed over the past decade and has already been used to increase the sensitivity of many axion search experiments [7,8]. The Center for Axion and Precision Physics Research (CAPP) recently implemented a flux-driven Josephson parametric amplifier (JPA) in the receiver chain of the axion haloscope, which reduced the noise of the system to the quantum regime. The flux-driven JPA is a quantum-noise-limited amplifier consisting of a superconducting quantum interference device (SQUID) at the end of a coplanar waveguide $\lambda/4$ resonator [9]. A dc magnetic flux through the SQUID loop tunes the resonant frequency of the JPA, while an inductively coupled pump tone is used to operate it in the three-wave mixing mode, which induces a parametric amplification [10,11]. While the JPA's limitations in instantaneous bandwidth make it difficult to realize its full potential for CAPP's experimental programs, its contribution to improving the overall system noise temperature is immense.

In this Letter, we report the recent results of a pilot axion-cavity experiment (CAPP-PACE), where a JPA was integrated into a conventional axion dark matter experiment to obtain the full benefit of a quantum-noise-limited amplifier. With the upgraded receiver chain, the experiment recorded the lowest noise among published axion haloscope searches under phase-insensitive operation, improving frequency scan speed by a factor of 50. We also introduced a newly developed scanning method which statistically optimizes the total scan time by dividing the scanning process into two steps. The new method has greatly improved the net scan speed, and more benefits could be obtained by using a cavity with a higher loaded quality factor [12].

The CAPP-PACE consists of a 1.12-L split-style copper cavity with a sapphire tuning rod, an 8-T NbTi superconducting magnet, and a cryogenic rf receiver chain with a flux-driven JPA, a major upgrade from the previous experiment [13]. It is critical to design the rf receiver chain so that it has the lowest possible noise temperature, as the scan speed is proportional to the inverse square of the system noise [14]. Figure 1 shows the new receiver chain with the JPA [9–11,15,16] as a preamplifier and the associated electronics. The JPA was sealed with a two-layer superconducting magnetic shield, and the shielded JPA was

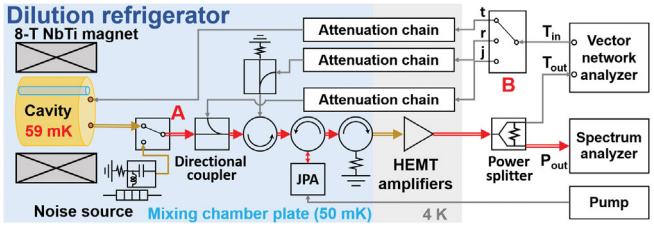

FIG. 1. Schematic of the JPA-implemented CAPP-PACE detector. At the 4 K stage, two HEMT amplifiers with 1.5 and 2.0 K of noise, respectively, are installed in series. With the same design as in the previous work [13], a noise source capable of precise temperature control is connected to one side of switch A, enabling a noise measurement of JPA and HEMT. Switch B connects the network analyzer's input signal and the ports for measuring cavity transmission (t), cavity reflection (r), and JPA characteristics (j). The arrows colored in yellow indicate NbTi superconducting line, while the rest of the lines were made of Cu or CuNi. The arrows with double lines show the mainstream chain.

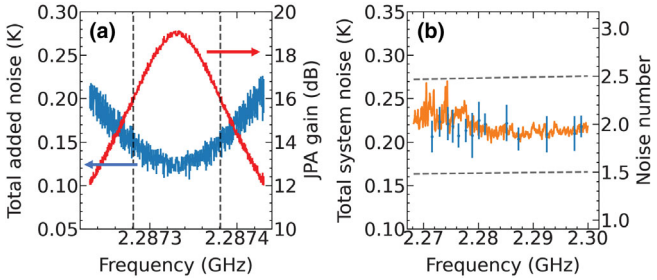

FIG. 2. (a) Measurement of the receiver chain noise. The blue curve is the total added noise, and the red curve is the JPA gain. The black dashed lines indicate the frequency window of the analysis (100 kHz). (b) Cross-check between the noise tracked during run A (orange solid line) and the reference noise using the modified Y-factor method (blue dots). The tracked noise was obtained from the experimental run's power spectra. The black dashed line is a contour of the noise number, which is a frequency-dependent value.

placed at the center of the mixing-chamber plate (MXC) of a dilution refrigerator, where the fringe magnetic field is the lowest (≈200 G). The magnetic flux penetration was less than 0.5 magnetic flux quanta, and the JPA gain was maintained with a fluctuation of less than 0.1 dB during the experiment.

The system noise of the haloscope receiver chain with JPA can be expressed as [10,13,17]

$$T_{\mathrm{sys}} = T_{\mathrm{phy}} + T_{\mathrm{add}}, \tag{1}$$

$$T_{\mathrm{add}} = (T_{\mathrm{JPA},i} + T_{\mathrm{JPA},e}) + \frac{T_{\mathrm{HEMT}}}{G_{\mathrm{JPA}}}. \tag{2}$$

T_{phy} is the quantum and the thermal noise of the cavity, defined as $T_{\mathrm{phy}} = h\nu/k_B[1/(e^{h\nu/k_B T_{\mathrm{cav}}} - 1) + 1/2]$, and T_{add} is the total added chain noise to T_{phy}. G_{JPA} and T_{JPA} are the gain and the noise of the JPA, respectively. JPA noise T_{JPA} consists of an idler term ($T_{\mathrm{JPA},i}$) and an extrinsic term ($T_{\mathrm{JPA},e}$). $T_{\mathrm{JPA},i}$ is the irreducible noise in the phase-insensitive operation and defines the quantum limit [18]. It is theoretically expected to be identical to T_{phy} multiplied by the attenuation between the cavity antenna and the JPA (≈1 dB) [13,17,19], if the cavity and MXC are in thermal equilibrium. $T_{\mathrm{JPA},e}$ is a collection of various noises that are generated by JPA operations. T_{HEMT} represents the noise generated in the post-JPA chain, where the HEMT noise is dominant.

In the cryogenic environment, the temperature of the MXC was controlled to be around 50 mK, achieving the stable operation of the JPA. The temperature of the cavity (T_{cav}) was 59 mK under the 8-T magnetic field, producing about 75 mK of physical noise (T_{phy}) in the frequency range near 2.3 GHz [20,21]. T_{HEMT} was measured to be 1.66 ± 0.06 K using the conventional Y-factor method [13,22,23] with the inactivated JPA.

To verify the JPA characteristics (T_{JPA} and G_{JPA}), a modified Y-factor method was applied at three input noise power levels (60, 120, and 180 mK). The added noise and the system gain were determined via fitting to the JPA-specific equation, including the dependency of $T_{\mathrm{JPA},i}$ on T_{phy} [10]. Figure 2(a) shows T_{add} and G_{JPA} of the receiver chain when the JPA resonant frequency was 2.2873 GHz and the JPA center gain was 19 dB. The estimated T_{add} at resonance was 129 ± 16 mK, and the system noise T_{sys} was correspondingly estimated to be 204 mK (see Table I). The extrinsic term of the JPA noise, $T_{\mathrm{JPA},e}$, was kept small (≈13 mK), and the number of noise photons [18] throughout the receiver chain was below 2 quanta. The JPA instantaneous bandwidth Δf_{JPA} was ∼100 kHz, which was wide enough to cover the cavity bandwidth. The measurement was repeated at various JPA resonant frequencies, by tuning the frequency with the dc magnetic flux. While tuning, $\Delta f_{\mathrm{JPA}} \geq 80$ kHz and $G_{\mathrm{JPA}} \geq 16$ dB were maintained by adjusting the pump tone. The noise

TABLE I. Noise contributions of the rf chain characterized at 2.2873 GHz. T_{phy}, T_{HEMT}, and T_{add} were measured directly, while T_{JPA} was decoupled from T_{add} by calculation. The total system noise T_{sys} was 204 mK, which corresponds to 1.87 quanta of the noise number. The dominant part of the errors in T_{HEMT} and T_{JPA} was from the fittings in the Y-factor method.

Noise contribution	Measurement at 2.2873 GHz
T_{phy}	75 ± 3 mK ($0.69 \times h\nu$)
$T_{\mathrm{HEMT}}/G_{\mathrm{JPA}}$	21 ± 1 mK ($0.19 \times h\nu$)
T_{JPA} ($= T_{\mathrm{JPA},i} + T_{\mathrm{JPA},e}$)	108 ± 15 mK ($0.99 \times h\nu$)
T_{sys} (total)	204 ± 16 mK ($1.87 \times h\nu$)

TABLE II. Major parameters of two experimental runs.

Experimental runs	Run A	Run B
Period (2020)[a]	Apr 01–May 11	Sep 05–Sep 18
Frequency range (GHz)	2.2704–2.3000	2.2705–2.2997
Axion mass m_a (μeV)	9.3906–9.5130	9.3910–9.5118
Frequency bin width	100 Hz	
Single tuning step	12 kHz	
Sweep time τ_0[b]	60 sec	
Number of spectra[c]	7	5
Sweep time per step τ[d]	7 min	5 min
Number of steps	2485	2455
Quality factor Q_0[e]	90 000	86 000
Magnetic field	7.2 T	
Cavity volume	1.12 L	
Geometrical factor	0.45	
MXC temperature	50 mK	
Cavity temperature	59 mK	79 mK
System noise T_{sys}[f]	220 mK	260 mK

[a]The time for maintenance is included.
[b]Pure sweep time without dead time.
[c]Number of spectra per step.
[d]$\tau =$ number of spectra per step $\times\tau_0$.
[e]Q_0 degradation comes from the oxidization of the cavity.
[f]Noise values are averaged over the total frequency range.

measurement results in 2.27–2.30 GHz range are plotted in Fig. 2(b) (blue dots).

Axion dark matter physics data were collected for the corresponding frequency range, with the parameters shown in Table II utilizing the data acquisition process described in a previous work [13,24]. There were two experimental runs, run A and run B. From both runs, a total of 4940 power spectra were collected, which covered the 2.2704–2.3000 GHz frequency range (corresponding to 9.39–9.51 μeV in mass units). The span size of the spectra was set to 2 MHz to cover the entire cavity resonance region, and the resolution bandwidth was set to 100 Hz for the multibin search so that the axion signal shape (∼1 kHz) was properly resolved. The frequency tuning step between the spectra in each run was 12 kHz, which was about $1/6$ of the cavity frequency bandwidth. The cavity frequency tuning was accomplished by rotating a sapphire rod through a piezoelectric actuator, followed by the tuning of the JPA's resonant frequency. Since this process changed the working point of the JPA, the power level of the spectrum and the gain of the system were examined to track the system noise. The changes in the system noise from the reference frequency (2.3 GHz) were compared, where the noise at the reference frequency was measured accurately using the modified Y-factor method. The average tracked system noise of run A was found to be 220 mK ($2.00 \times h\nu$), which was consistent with the noise values from the Y-factor measurement [see Fig. 2(b)]. The average system noise in run B increased to 260 mK ($2.35 \times h\nu$), mainly due to the poor thermal contact between the cavity and the MXC plate.

The analysis procedure was essentially the same as in the previous experiments [8,13,25,26]. The analysis began with the removal of the baseline in the power spectrum, which contained the effect of the frequency-dependent gain [10] and impedance mismatch of the receiver chain [27]. The shape of the power spectrum baseline was estimated using the Savitzky-Golay filter [28] and extracting it from the original spectrum restored the normal distribution of the noise profile. Conducting an optimization of the filter parameters [29] with a Monte Carlo simulation, the signal reduction due to the baseline removal was minimized to around 20%, when the polynomial order d was 5 and the window length $2W + 1$ was 391. Next, a process called "combination" [26] completed the construction of a grand spectrum over the entire scan range by convolving the noise-normalized axion line shape and the baseline-removed data [30]. The axion velocity dispersion with respect to the Galactic Center was set to 270 km/s, and 230 km/s was used for the orbital speed of the Sun around the Galaxy [31].

The final step in the analysis was to define and examine axion candidates using a threshold-based criterion, where a threshold for axion candidates was defined using a signal-to-noise ratio (SNR) and a confidence level. Conventionally, once a target sensitivity level $g_{a\gamma\gamma}$ and a target SNR (usually 5) are set, the total scan time $\Delta t_{\mathrm{total}}$ can be determined based on the experimental parameters [8,26]. To reduce $\Delta t_{\mathrm{total}}$, we developed a two-stage scanning method which splits the conventional scan into two scans and inserts an intermediate threshold between scans. The initial scan first sweeps the entire frequency range with the preset $g_{a\gamma\gamma}$ and the intermediate SNR less than 5. A second scan is then performed over those surviving frequency bins. The second scan data are collected with enough integration time to make the final SNR become 5, when merged with the initial scan. From the combined data, axion candidates are determined using the final threshold of SNR 5. In this way, unlike the conventional scan, not all frequency bins are investigated until the SNR reaches 5, which reduces the total scan time without changing the final confidence level.

To determine the optimal value of the intermediate SNR and minimize the total scan time, a Monte Carlo simulation was conducted with various intermediate SNR values, aiming for 90% confidence. However, due to the presence of noise in both scans, more than 10% of the true axion signal can be rejected, if the confidence level for each scan is set to 90%. To overcome this problem, a slightly higher confidence level was set for each rejection criterion, by lowering the level of the threshold. A threshold level obtained from numerical calculations was used to control the net confidence to 90%, which was also verified by the simulation. Figure 3(a) shows how much scan time could be saved by having an intermediate SNR when $g_{a\gamma\gamma}$ was fixed. Meanwhile, the efficiency of the second scan increased as the loaded quality factor of the cavity, Q_L,

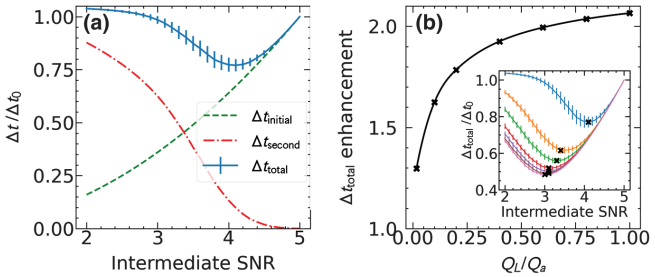

FIG. 3. (a) Simulation of the total scan time Δt_{total} as a function of the intermediate SNR, when applying a two-stage scanning method with a cavity that has a loaded quality factor of 30 000. The time unit is normalized to the scan time of the conventional scan, Δt_0, and Δt_{total} is given as a sum of $\Delta t_{\text{initial}}$ and Δt_{second}. The error bars indicate statistical errors by the stochastic behavior of the second scan. (b) Enhancement in the scan speed with respect to the loaded quality factor of the cavity, Q_L, which is normalized to the quality factor of the axion, Q_a. The inset shows the simulation results using the same method as in (a) but with various Q_L values. The markers in the inset indicate the optimized points that correspond to the markers in the main plot.

approached the axion quality factor Q_a, since the cavity with high Q_L has a bandwidth that can concentrate more on the surviving bins in the second scan. The enhancement of Δt_{total} with increasing Q_L is presented in Fig. 3(b). For the cavity used in this experiment [blue in Figs. 3(a) and 3(b)], Δt_{total} was found to be at minimum when the intermediate SNR was around 4.1, and the enhancement in scan speed was as much as ~30%. If the superconducting cavity [12] is utilized so that Q_L matches Q_a, the scan speed could be boosted up to 105%.

In the analysis of this experiment, the combined data of run *A* and run *B* formed the initial scan, and the optimal intermediate SNR for this experiment was found to be 4.2. There were a total of 1168 surviving frequency bins from the initial scan, which is close to the analytically expected number. When the data from the initial and the second scans were combined according to the two-stage scanning method, 46 axion candidates were found from the surviving bins. After a rescan with sufficiently high statistics, the candidates were completely excluded with the 90% confidence level. The actual improvement in scan speed by applying the two-stage scanning method was found out to be around 26%, similar to the simulation result. Assuming that the axion portion of dark matter for our local Galactic halo is 100%; i.e., $\rho_a = 0.45\ \text{GeV/cm}^3$, we obtained a coupling sensitivity of 2.7-fold above the Kim-Shifman-Vainshtein-Zakharov (KSVZ) level (see Fig. 4).

In conclusion, we report the first result of an axion haloscope search using a quantum-noise-limited JPA at CAPP. By implementing the JPA in the cryo-rf receiver chain, it was possible to reduce the total system noise down to approximately 200 mK in the 2.27–2.30 GHz frequency region, which is less than twice the standard quantum limit. We were able to achieve the lowest system noise recorded among published axion cavity haloscope searches under phase-insensitive operations, in terms of both the absolute temperature and the noise photon number. Thanks to the new receiver chain, the scan speed was improved by about a factor of 50 compared to the case with an inactivated JPA. In addition, a new scanning method was developed, which boosted the scan speed by ~26%. It is expected that this can be enhanced even more when a superconducting cavity is implemented in future work. As a result, we were able to exclude the $9.39 < m_a < 9.51$ μeV axion mass range with an order higher sensitivity than the existing limit, where the parameters are in the plausible model for the QCD axion [45,46].

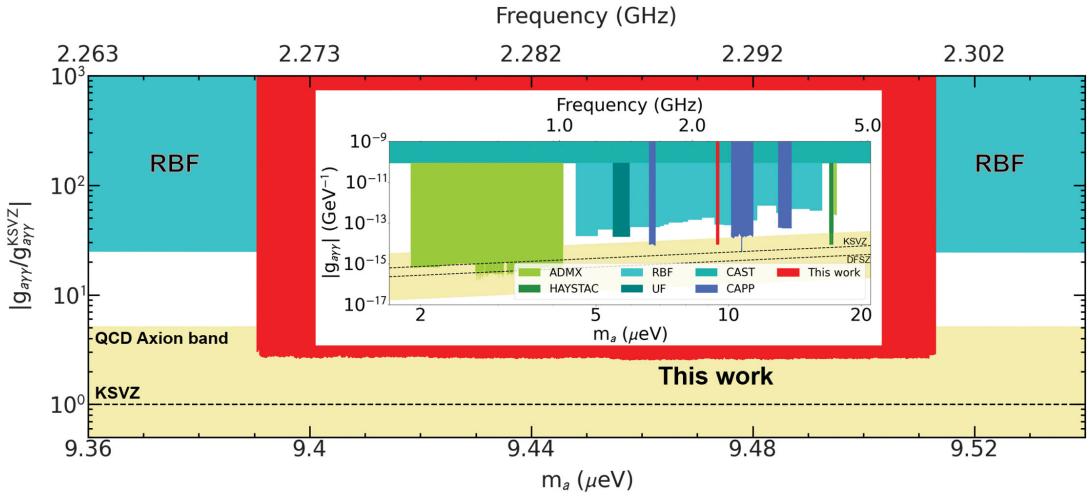

FIG. 4. Exclusion limit of this Letter at 90% confidence (red area). The inset shows this Letter along with other axion search results in the extended axion mass range [7,25,32–44]. The results from CAPP except this Letter are colored blue [13,26,30]. The yellow area shows the model band of QCD axion [45,46].

This work is supported in part by the Institute for Basic Science (IBS-R017-D1-2022-a00) and JST ERATO (Grant No. JPMJER1601). A. Ferdinand van Loo was supported by a JSPS postdoctoral fellowship.

*Corresponding author.
gnuhcw@ibs.re.kr

[1] R. D. Peccei and H. R. Quinn, CP Conservation in the Presence of Pseudoparticles, Phys. Rev. Lett. **38**, 1440 (1977).
[2] R. Bradley, J. Clarke, D. Kinion, L. J. Rosenberg, K. van Bibber, S. Matsuki, M. Mück, and P. Sikivie, Microwave cavity searches for dark-matter axions, Rev. Mod. Phys. **75**, 777 (2003).
[3] P. A. R. Ade *et al.* (Planck Collaboration), Planck 2015 results—XIII. Cosmological parameters, Astron. Astrophys. **594**, A13 (2016).
[4] J. E. Kim, Weak-Interaction Singlet and Strong *CP* Invariance, Phys. Rev. Lett. **43**, 103 (1979); M. Shifman, A. Vainshtein, and V. Zakharov, Can confinement ensure natural *CP* invariance of strong interactions?, Nucl. Phys. **B166**, 493 (1980); J. E. Kim, Light pseudoscalars, particle physics and cosmology, Phys. Rep. **150**, 1 (1987).
[5] A. R. Zhitnitsky, On possible suppression of the axion hadron interactions. (In Russian), Yad. Fiz. **31**, 497 (1980) [Sov. J. Nucl. Phys. **31**, 260 (1980)]; M. Dine, W. Fischler, and M. Srednicki, A simple solution to the strong *CP* problem with a harmless axion, Phys. Lett. **104B**, 199 (1981).
[6] P. Sikivie, Experimental Tests of the "Invisible" Axion, Phys. Rev. Lett. **51**, 1415 (1983).
[7] S. J. Asztalos, G. Carosi, C. Hagmann, D. Kinion, K. van Bibber, M. Hotz, L. J. Rosenberg, G. Rybka, J. Hoskins, J. Hwang, P. Sikivie, D. B. Tanner, R. Bradley, and J. Clarke, Squid-Based Microwave Cavity Search for Dark-Matter Axions, Phys. Rev. Lett. **104**, 041301 (2010).
[8] B. Brubaker, L. Zhong, Y. Gurevich, S. Cahn, S. Lamoreaux, M. Simanovskaia, J. Root, S. Lewis, S. Al Kenany, K. Backes *et al.*, First Results from a Microwave Cavity Axion Search at 24 μeV, Phys. Rev. Lett. **118**, 061302 (2017).
[9] T. Yamamoto, K. Inomata, M. Watanabe, K. Matsuba, T. Miyazaki, W. D. Oliver, Y. Nakamura, and J. S. Tsai, Flux-driven Josephson parametric amplifier, Appl. Phys. Lett. **93**, 042510 (2008).
[10] Ç. Kutlu, A. F. van Loo, S. V. Uchaikin, A. N. Matlashov, D. Lee, S. Oh, J. Kim, W. Chung, Y. Nakamura, and Y. K. Semertzidis, Characterization of a flux-driven Josephson parametric amplifier with near quantum-limited added noise for axion search experiments, Supercond. Sci. Technol. **34**, 085013 (2021).
[11] S. Uchaikin, A. Matlashov, D. Lee, W. Chung, S. J. Oh, Y. Semertzidis, V. Zakosarenko, Ç. Kutlu, A. van Loo, Y. Urade *et al.*, Development of SQUID amplifiers for axion search experiments, in *Proceedings of the 2019 IEEE International Superconductive Electronics Conference (ISEC)* (IEEE, New York, 2019), pp. 1–3.
[12] D. Ahn, O. Kwon, W. Chung, W. Jang, D. Lee, J. Lee, S. W. Youn, H. Byun, D. Youm, and Y. K. Semertzidis, Biaxially Textured YBa_2 Cu_3 $O_7 - x$ Microwave Cavity in a High Magnetic Field for a Dark-Matter Axion Search, Phys. Rev. Appl. **17**, L061005 (2022).
[13] O. Kwon, D. Lee, W. Chung, D. Ahn, H. S. Byun, F. Caspers, H. Choi, J. Choi, Y. Chung, H. Jeong *et al.*, First Results from an Axion Haloscope at CAPP around 10.7 μeV, Phys. Rev. Lett. **126**, 191802 (2021).
[14] L. Krauss, J. Moody, F. Wilczek, and D. E. Morris, Calculations for Cosmic Axion Detection, Phys. Rev. Lett. **55**, 1797 (1985).
[15] L. Zhong *et al.*, Squeezing with a flux-driven Josephson parametric amplifier, New J. Phys. **15**, 125013 (2013).
[16] S. Pogorzalek *et al.*, Hysteretic Flux Response and Nondegenerate Gain of Flux-Driven Josephson Parametric Amplifiers, Phys. Rev. Appl. **8**, 024012 (2017).
[17] H. T. Friis, Noise figures of radio receivers, Proc. IRE **32**, 419 (1944).
[18] C. M. Caves, Quantum limits on noise in linear amplifiers, Phys. Rev. D **26**, 1817 (1982).
[19] R. H. Dicke, The measurement of thermal radiation at microwave frequencies, in Classics in Radio Astronomy (Springer, New York, 1946), pp. 106–113.
[20] J. B. Johnson, Thermal agitation of electricity in conductors, Phys. Rev. **32**, 97 (1928).
[21] H. Nyquist, Thermal agitation of electric charge in conductors, Phys. Rev. **32**, 110 (1928).
[22] G. F. Engen, A new method of characterizing amplifier noise performance, IEEE Trans. Instrum. Meas. **19**, 344 (1970).
[23] M. Leffel and R. Daniel, The Y factor technique for noise figure measurements, Technical Report No. 1MA178_5e, Rohde & Schwartz, 2011.
[24] S. Lee, Development of a data acquisition software for the cultask experiment, J. Phys. **898**, 032035 (2017).
[25] C. Hagmann, D. Kinion, W. Stoeffl, K. vanBibber, E. Daw *et al.*, Results from a High-Sensitivity Search for Cosmic Axions, Phys. Rev. Lett. **80**, 2043 (1998).
[26] S. Lee, S. Ahn, J. Choi, B. R. Ko, and Y. K. Semertzidis, Axion Dark Matter Search Around 6.7 μeV, Phys. Rev. Lett. **124**, 101802 (2020); J. Jeong, S. W. Youn, S. Bae, J. Kim, T. Seong, J. E. Kim, and Y. K. Semertzidis, Search for Invisible Axion Dark Matter with a Multiple-Cell Haloscope, Phys. Rev. Lett. **125**, 221302 (2020).
[27] S. Asztalos, E. Daw, H. Peng, L. J. Rosenberg, C. Hagmann *et al.*, Large-scale microwave cavity search for dark-matter axions, Phys. Rev. D **64**, 092003 (2001).
[28] R. W. Schafer, Report, Technical Report No. HPL-2010-109, HP Laboratories, 2010.
[29] B. M. Brubaker, L. Zhong, S. K. Lamoreaux, K. W. Lehnert, and K. A. van Bibber, Haystac axion search analysis procedure, Phys. Rev. D **96**, 123008 (2017).
[30] G. Turin, An introduction to matched filters, IRE Trans. Inf. Theory **6**, 311 (1960).
[31] M. S. Turner, Periodic signatures for the detection of cosmic axions, Phys. Rev. D **42**, 3572 (1990).
[32] S. DePanfilis, A. C. Melissinos, B. E. Moskowitz, J. T. Rogers, Y. K. Semertzidis, W. U. Wuensch, H. J. Halama, A. G. Prodell, W. B. Fowler, and F. A. Nezrick, Limits on

the Abundance and Coupling of Cosmic Axions at $4.5 < m_a < 5.0$ μeV, Phys. Rev. Lett. **59**, 839 (1987).
[33] W. U. Wuensch, S. De Panfilis-Wuensch, Y. K. Semertzidis, J. T. Rogers, A. C. Melissinos, H. J. Halama, B. E. Moskowitz, A. G. Prodell, W. B. Fowler, and F. A. Nezrick, Results of a laboratory search for cosmic axions and other weakly coupled light particles, Phys. Rev. D **40**, 3153 (1989).
[34] C. Hagmann, P. Sikivie, N. S. Sullivan, and D. B. Tanner, Results from a search for cosmic axions, Phys. Rev. D **42**, 1297 (1990).
[35] S. J. Asztalos *et al.*, Experimental constraints on the axion dark matter halo density, Astrophys. J. **571**, L27 (2002).
[36] S. J. Asztalos *et al.*, Improved rf cavity search for halo axions, Phys. Rev. D **69**, 011101(R) (2004).
[37] C. Boutan *et al.* (ADMX Collaboration), Piezoelectrically Tuned Multimode Cavity Search for Axion Dark Matter, Phys. Rev. Lett. **121**, 261302 (2018).
[38] N. Du *et al.* (ADMX Collaboration), Search for Invisible Axion Dark Matter with the Axion Dark Matter Experiment, Phys. Rev. Lett. **120**, 151301 (2018).
[39] T. Braine *et al.* (ADMX Collaboration), Extended Search for the Invisible Axion with the Axion Dark Matter Experiment, Phys. Rev. Lett. **124**, 101303 (2020).
[40] C. Bartram, T. Braine, E. Burns, R. Cervantes, N. Crisosto, N. Du, H. Korandla, G. Leum, P. Mohapatra, T. Nitta *et al.*, Search for Invisible Axion Dark Matter in the 3.3–4.2 μeV Mass Range, Phys. Rev. Lett. **127**, 261803 (2021).
[41] M. Arik *et al.* (CAST Collaboration), New solar axion search using the CERN Axion Solar Telescope with ^{4}He filling, Phys. Rev. D **92**, 021101 (2015).
[42] V. Anastassopoulos *et al.* (CAST Collaboration), New cast limit on the axion–photon interaction, Nat. Phys. **13**, 584 (2017).
[43] L. Zhong, S. Al Kenany, K. M. Backes, B. M. Brubaker, S. B. Cahn, G. Carosi, Y. V. Gurevich, W. F. Kindel, S. K. Lamoreaux, K. W. Lehnert *et al.*, Results from phase 1 of the haystac microwave cavity axion experiment, Phys. Rev. D **97**, 092001 (2018).
[44] K. Backes, D. A. Palken, S. Al Kenany, B. M. Brubaker, S. Cahn, A. Droster, G. C. Hilton, S. Ghosh, H. Jackson, S. K. Lamoreaux *et al.*, A quantum enhanced search for dark matter axions, Nature (London) **590**, 238 (2021).
[45] R. D. Peccei, The strong *CP* problem and axions, in *Axions* (Springer, New York, 2008), pp. 3–17.
[46] S. L. Cheng, C. Q. Geng, and W.-T. Ni, Axion-photon couplings in invisible axion models, Phys. Rev. D **52**, 3132 (1995).